Two-dimensional cyclotron-resonance maser array: Spectral measurements with one and two electron beams

Li Lei and Eli Jerby*
Faculty of Engineering, Tel Aviv University, Ramat Aviv 69978, Israel
(Received 8 September 1997; revised manuscript received 17 September 1998)

The cyclotron-resonance-maser (CRM) array is a device in which separate electron beams perform simultaneously a cyclotron interaction with a single Bloch wave in an artificial lattice. The CRM array has the capability of generating high-power microwaves with relatively low-voltage electron beams. The low-voltage operation reduces the system overhead and leads to a relatively compact device. In future schemes, the CRM array may radiate directly to free space as an *active* phased-array antenna. Furthermore, the phase of each element output, and therefore the antenna far-field radiation pattern, can be varied by the electron-beam voltages. This paper presents an experimental demonstration of a CRM array. In this experiment, a two-dimensional CRM array is operated with one and two electron beams (~10 keV, 0.1 A each). Microwave output signals are observed in frequencies around 7 GHz in an axial magnetic field of ~3 kG. Spectral measurements of the CRM outputs reveal frequency sweeps along the CRM pulses. These are associated with electron-energy variations, in accordance with the theoretical CRM tuning condition. The synchronism of the cyclotron-resonance interaction with a backward spatial harmonic is confirmed. These results promote the efforts toward the realization of large CRM arrays. [S1063-651X(99)02002-4]

PACS number(s): 41.60.−m, 84.40.Ik, 52.35.Qz, 52.35.Hr

I. INTRODUCTION

Cyclotron-resonance masers (CRMs) and gyrotrons [1,2] have been developed so far as *single-electron-beam* tubes. In order to obtain high output power, the sole electron beam should possess sufficiently large kinetic energy and current. Consequently, a major part of the *overhead* in a typical CRM system is devoted to peripheral accessories needed to maintain the powerful electron beam itself in both the acceleration and the collector sections. In fact, most of the total length of a typical gyrodevice is devoted to the consequent overhead (including the high-voltage electron gun and electron optics, the tube shielding, a long collector, and the output window).

The concept of multibeam CRM arrays was proposed [3,4] as a compact version of the single-beam CRM schemes. In the CRM array, separate electron beams perform simultaneously a cyclotron interaction with a single Bloch wave in an artificial lattice. The CRM array has the capability of generating high-power microwaves with relatively low operating voltages. A theoretical analysis of the CRM array [5] predicts a considerable gain in a single mode. The mode selectivity and spectral purity in this device stem from the spatial filtering in the periodic structure. In addition, the CRM array may have unique features of an *active* phased array antenna [6]. The immediate integration proposed, of a microwave generator combined with an antenna, may simplify the overall radiative system in many applications.

Other types of microwave generators with more than one electron beam have been proposed and studied by other workers. These include the multiple-beam klystron [7], the cluster klystron for linear colliders [8], the double-stream cyclotron maser [9], and the multibeam stagger-tuned gyroklystrons [10].

The CRM array can be classified as a slow-wave cyclotron maser, unlike typical single-beam gyrodevices, such as gyrotrons, cyclotron autoresonance masers, and their derivatives, which are fast-wave devices. Slow-wave CRMs, such as dielectric-loaded devices [11–13], have been studied to a lesser extent. In general, the CRM interaction involves azimuthal and axial bunching effects. The fast-wave CRMs are dominated by the relativistic azimuthal bunching, while slow-wave CRMs (operating in the Weibel regime) are dominated by the axial bunching effect [14]. A periodic waveguide acts as an artificial dielectric loading for the CRM interaction. The electron beam, rotating in a uniform axial magnetic field, interacts then with a spatial harmonic of the periodic waveguide. The cyclotron resonance condition

$$\omega = \omega_c + \beta_n v_z \tag{1}$$

determines the CRM tuning, where ω and β_n are the electromagnetic (em) -wave frequency and wave number of the nth-order spatial harmonic, respectively, $\omega_c = eB_0/\gamma m$ is the electron cyclotron frequency, v_z and γ are the electron axial velocity and relativistic factor, respectively, and B_0 is the static magnetic field. Periodic-waveguide CRM devices (including the CRM array studied in this paper) may operate with either slow or fast waves, according to their actual tuning condition with respect to the waveguide dispersion.

This paper presents an experimental study of a two-dimensional (2D) CRM array with one and two electron beams. The following sections describe the concept in general, the setup used in this experiment, and spectral measurement results that show clearly the CRM interaction with backward spatial harmonics. Both fast- and slow-wave CRM interactions are observed in this experiment.

*Author to whom correspondence should be addressed. Electronic address: jerby@eng.tau.ac.il

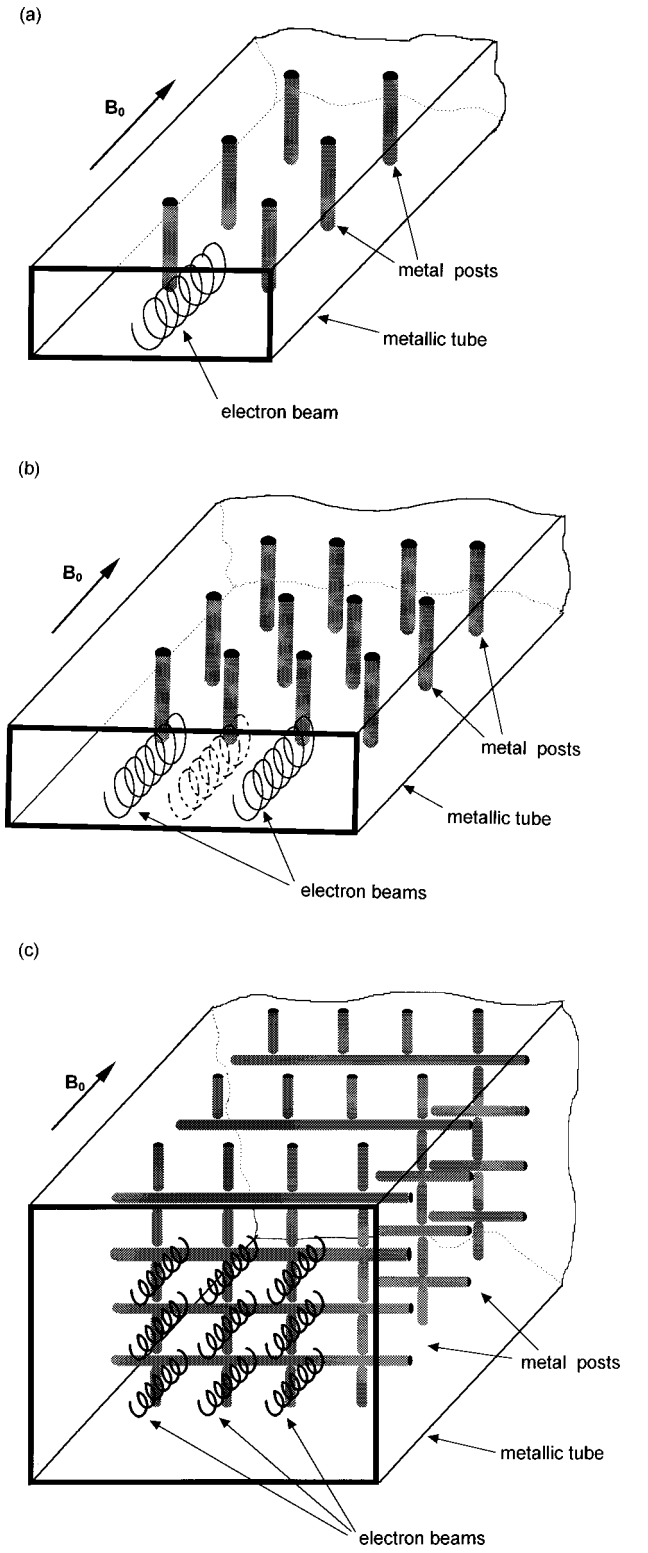

FIG. 1. Evolution of the CRM-array concept: Examples of (a) 1D, (b) 2D, and (c) 3D CRM-array schemes.

II. THE CRM-ARRAY CONCEPT

The CRM array has been evolved as an extension of the periodic-waveguide CRM scheme shown in Fig. 1(a) [15,16]. In this device, referred to here as a 1D CRM array, the waveguide consists of metal posts in two columns, with the electron beam flowing in between them. Theoretical studies of 1D CRM interactions with slow and fast waves are

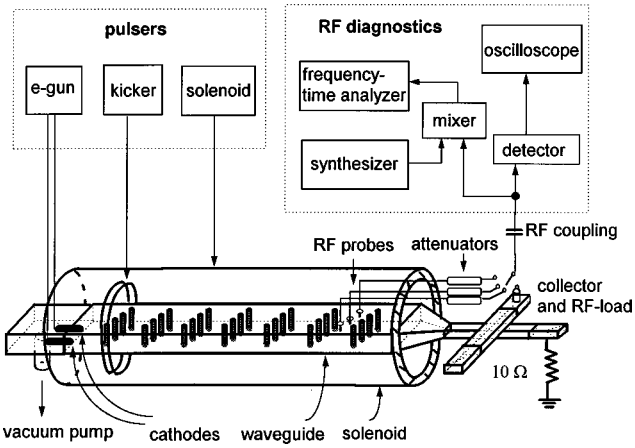

FIG. 2. Schematic of the 2D CRM-array experimental setup.

presented in Refs. [17,18]. Amplifier and oscillator experiments were conducted at *X*-band frequencies (8–12 GHz) with electron beams of ~10 keV. The 1D CRM oscillator [16] yielded a coherent output of 0.4-kW power at greater than 25% efficiency. A direct scaling up of this 1D scheme to high power levels might have required a system overhead comparable to that of similar single-beam gyrotrons. The preferred alternative in this study is to increase the device *dimensionality*.

Conceptual schemes of 2D and 3D CRM arrays are illustrated, for example, in Figs. 1(b) and 1(c), respectively. The CRM array consists of many 1D CRM channels, each operating with a low-voltage, low-perveance electron beam. The different channels may be strongly coupled together through the waveguide lattice. Synergistic effects between these channels may increase the output power further. In order to compensate for any transverse nonuniformity in the magnetic field profile, each electron beam can be tuned to a slightly different accelerating voltage.

The ultimate 3D CRM array may consist of tens and even hundreds of electron beams. Advanced cathode arrays, made of carbon fibers, silicon tips, or ferroelectric ceramics, could be applicable in this device. The radiation output can be

TABLE I. Experimental parameters.

Parameter	Value
Electron beams	
Energy (keV)	4.0–10.5
Beam current (A)	~0.1
Pulse duration (ms)	0.2
Beams	1 or 2
Magnetic fields	
Solenoid (kG)	2.5–3.9
Kicker (kA turns)	~0.7
Periodic waveguide	
Rectangular tube (mm^2)	48×22
Length (cm)	48
Post diameter (mm)	1.5
Array size	4×24
Periodicity (mm)	20

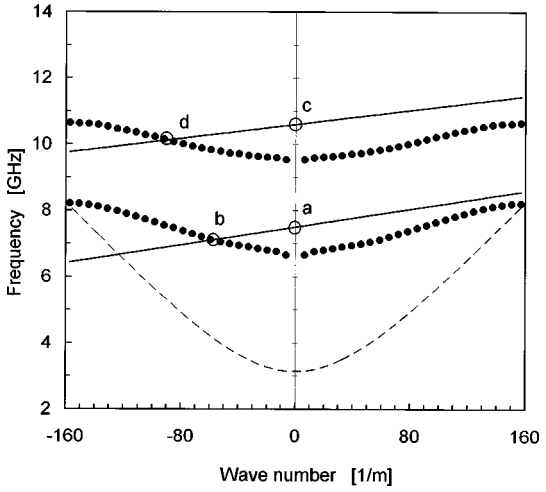

FIG. 3. Measured Brillouin diagram of the 2D periodic waveguide (the dots indicate measurement points). The solid beam lines represent Eq. (1) in different cyclotron frequencies (points *a* and *c*). The dashed curve shows the fundamental mode of the (empty) rectangular tube.

emitted from the exit plane of the CRM array directly to free space. In more sophisticated schemes, the CRM array may have features of an active phased-array antenna. Focusing, steering, and splitting of the radiation lobe could be manipulated by varying the voltage profile across the cathode array [6]. The major advantages expected for the CRM-array concept are (a) compact size and small system overhead due to the low-voltage operation and the relatively large effective volume and wide transverse cross section, (b) reduced space-charge effects due to the separated low-current electron beams, (c) spectral purity and mode selectivity determined by the lattice dispersion, and (d) direct radiation to free space.

III. EXPERIMENTAL SETUP

A block diagram of the 2D CRM-array experimental setup [19] is shown in Fig. 2. The oscillator tube consists of planar electron guns, a 2D periodic waveguide, a solenoid, and a kicker coil. The device is activated by pulsed power supplies as described in Ref. [16]. The CRM device is immersed in a uniform axial magnetic field (2–4 kG). The electron beams are emitted from dispenser thermionic cathodes (Spectra-Mat, STD 200, 5 mm in diameter), spun up by the small kicker coil, and propagate in cyclotron motions along the periodic waveguide channels. The waveguide consists of a metal-post array with 4×24 elements. The first row of metal posts acts as an anode. A waveguide taper at the end is used as a mode converter and also as a collector for the electron beams. In another scheme (not presented here) the collector is divided between each electron beam. The beam currents are measured by means of 10-Ω resistors. A small portion of the rf power is sampled by a 20-dB cross coupler and three sampling probes. The output coupled rf signal is attenuated and divided into two arms. In one arm, the signal is detected by a high-sensitivity crystal detector [Hewlett-Packard (HP) model No. 424A] and recorded by a digital oscilloscope (Tektronix TDS 540). In the other arm, the signal is fed into a mixer (HP 5364A) and mixed with a local-oscillator wave generated by a synthesizer (HP 83752A). The heterodyne signal is analyzed by a frequency and time-interval analyzer (HP 5372A), which enables intrapulse frequency variation measurements. The parameters of the 2D

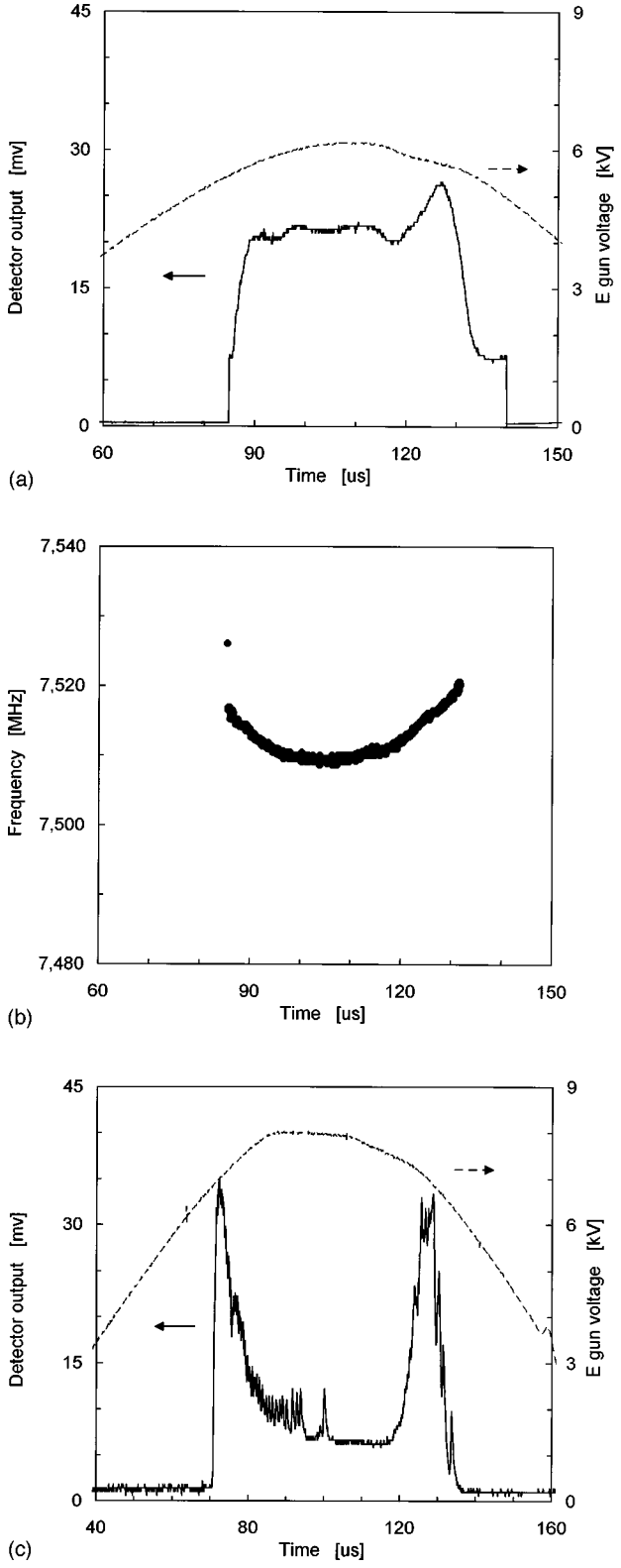

FIG. 4. Experimental results of the one-beam CRM oscillator at 2.9 kG: (a) the detector rf output (solid line) and the electron-gun voltage (dashed line), (b) the frequency variation during the pulse, and (c) an off-tuned operation at 2.7 kG.

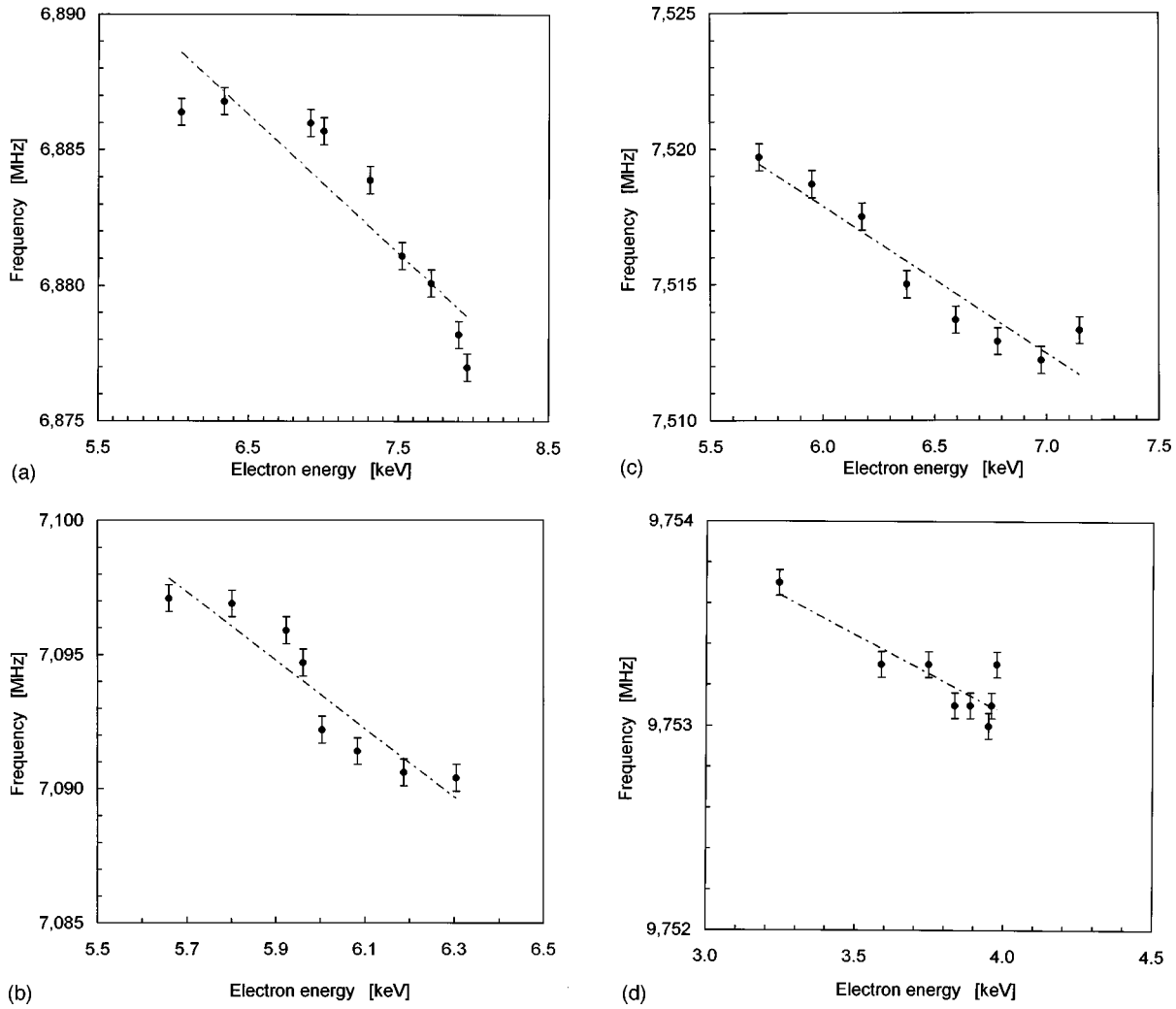

FIG. 5. Tuning characteristics of a one-beam CRM at (a) 2.6 kG, (b) 2.7 kG, (c) 2.9 kG, and (d) 3.7 kG.

CRM-array experiment are listed in Table I.

The waveguide dispersion (without electron beams) is shown in a Brillouin diagram in Fig. 3, as results from measurements of the waveguide reflection and transmission coefficients by a scalar network analyzer (HP 8757A). Using the method described in Refs. [16,20,21], the minima in the reflection trace present the resonance frequencies of the finite periodic waveguide and satisfy the resonance condition

$$\phi_s = \beta_s L = s\pi, \quad s = 1,2,\ldots,24, \tag{2}$$

where L is the waveguide length. The dispersion curve is constructed by fitting the measured frequencies of the reflection minima and the discrete wave numbers that result from Eq. (2). These intersections are shown by the dots in Fig. 3.

Electron beam lines (1) are added to Fig. 3 in order to demonstrate CRM interactions in different cyclotron frequencies (points *a* and *c*). The intersections with the waveguide dispersion curves (points *b* and *d*) indicate a possible CRM interaction with backward waves in different frequency passbands. Forward- and backward-wave interactions ($\beta_n > 0$ and $\beta_n < 0$, respectively) differ by the tendency of the latter to act as absolute instabilities and to oscillate [22] (as observed in this experiment). The backward-wave interaction could be the desired mode for a CRM-array *oscillator*. In amplifier schemes, however, parasitic backward-wave interactions must be suppressed or eliminated by a proper tuning to a tangential (grazing) point in Fig. 3. The 2D CRM-array operation with one and two electron beams is presented in the next section.

IV. EXPERIMENTAL RESULTS

The 2D CRM-array experiment has been operated with one and two electron beams, as illustrated in Fig. 1(b) by dashed and solid curves, respectively. A single electron beam in the center channel yields the results shown in Figs. 4(a)–4(c). The detector output trace is presented in Fig. 4(a), together with the electron-beam energy trace. The frequency characteristic of the rf output signal is shown in Fig. 4(b) as measured during the pulse (the dots present the points of measurement). The axial magnetic field in this run is 2.9 kG, which corresponds to a cyclotron frequency of 8.0 GHz. The current measured in the collector is ~0.1 A. The average radiation frequency is 7.5 GHz, hence the device operates with a backward wave. This effect is clearly observed in Figs. 4(a) and 4(b) by the curvatures of the voltage and frequency traces (note that in a backward-wave interaction the frequency decreases as the electron energy increases). A slightly higher electron energy results in a ''rabbit-ears''

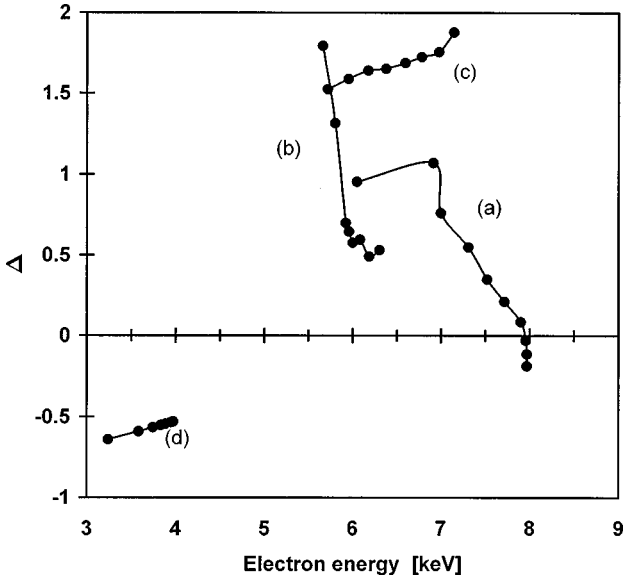

FIG. 6. Mismatch parameter Δ [Eq. (3)]. The curves denoted $a-d$ correspond to the results in Figs. 5(a)–5(d), respectively.

shape of the detector output, as shown in Fig. 4(c). The optimal resonance in this tuning condition is satisfied below the maximum voltage.

Single-beam measurements have been made in a wide range of axial magnetic fields and electron-gun voltages. Oscillations were observed in different frequencies as shown in Figs. 5(a)–5(d). In all cases, the frequency tends to decrease as the electron energy increases. For axial magnetic fields in the range 2.6–2.9 kG [Figs. 5(a)–5(c)], the corresponding wave frequency varies within 6.87–7.52 GHz, respectively, in the first passband of the periodic waveguide. For an axial magnetic field of 3.7 kG, interactions were observed in the second passband (9.75 GHz), as shown in Fig. 5(d). In the second passband, the coupling is much smaller since the interaction occurs mostly with the second transverse mode, which has a null in the center [5]. The emission in this case may result from the finite width of the electron beam or from its slightly off-axis propagation.

The agreement between the experimental results [Figs. 5(a)–5(d)] and the theoretical tuning relation [Eq. (1) and Fig. 3] can be evaluated by a mismatch parameter proposed as

$$\Delta=\left[\frac{\beta_0(\omega)v_0}{\omega_c-\omega}\right]^2-1. \tag{3}$$

This parameter is computed using the measured experimental data [i.e., the wave number $\beta_0(\omega)$, the total electron velocity v_0, and the cyclotron frequency ω_c are computed by the instantaneous em frequency, electron-gun voltage, and solenoid current, respectively]. Equations (1) and (3) show that $\Delta=(v_\perp/v_z)^2$, where $v_\perp$ is the initial electron transverse velocity. Hence the expected value for Δ is on the order of one [5] due to the actual $v_\perp$ induced by the kicker (note that $v_\perp$ is not measured in this experiment). Figure 6 shows the results of Δ computed by Eq. (3) for the experimental runs presented in Figs. 5(a)–5(d), respectively. Negative values of Δ in Fig. 6 can be attributed to the error range of the solenoid field measurement ($\sim$2%) and to the high sensitivity of Eq. (3) to the cyclotron frequency (note that $\omega_c\sim\omega$). Nevertheless, a result of $-0.7<\Delta<1.9$ indicates a reasonable agreement between experiment and theory.

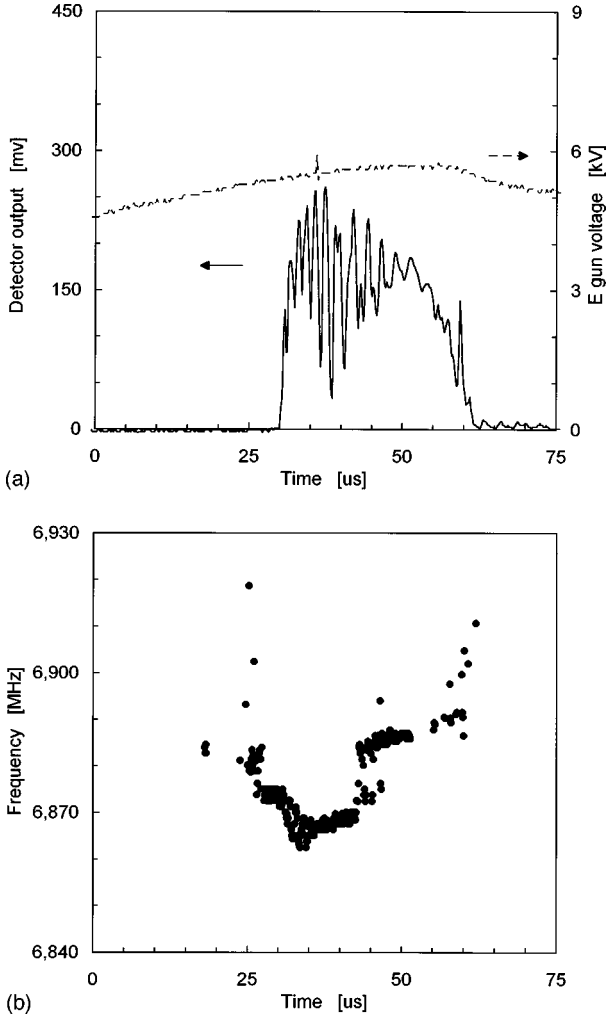

FIG. 7. 2D CRM-array operation with a single beam in an off-axis side channel at 2.7 kG: (a) the detector rf output (solid line) and the electron-gun voltage (dashed line) and (b) the frequency variation during the pulse.

The CRM array was operated also with a single electron beam in the side channel. A typical result for a 2.7-kG magnetic field is presented in Fig. 7. The extracted power of the rf sample by the various couplers in all the single-beam measurements was in the range 5–25 W. This power level is sufficient for spectral measurements.

The 2D CRM array was operated with two electron beams as shown in Fig. 1(b). Typical curves of the detector output and the electron-gun voltage pulse are shown in Fig. 8(a). A frequency variation of the rf output signal is shown in Fig. 8(b). The axial magnetic field in this run is 2.7 kG, which corresponds to a cyclotron frequency of 7.5 GHz. The average radiation frequency is 6.9 GHz, hence the device operates again in the backward-wave regime. In a CRM operation with an electron energy slightly higher than the optimal value, the synchronism condition takes place in the leading and trailing edges of the voltage pulse, as shown in Fig. 8(c).

By increasing the axial magnetic field, the two-beam CRM oscillates also at 3.8 kG. Figures 9(a) and 9(b) show the electron-gun voltage, the detector output, and the intra-

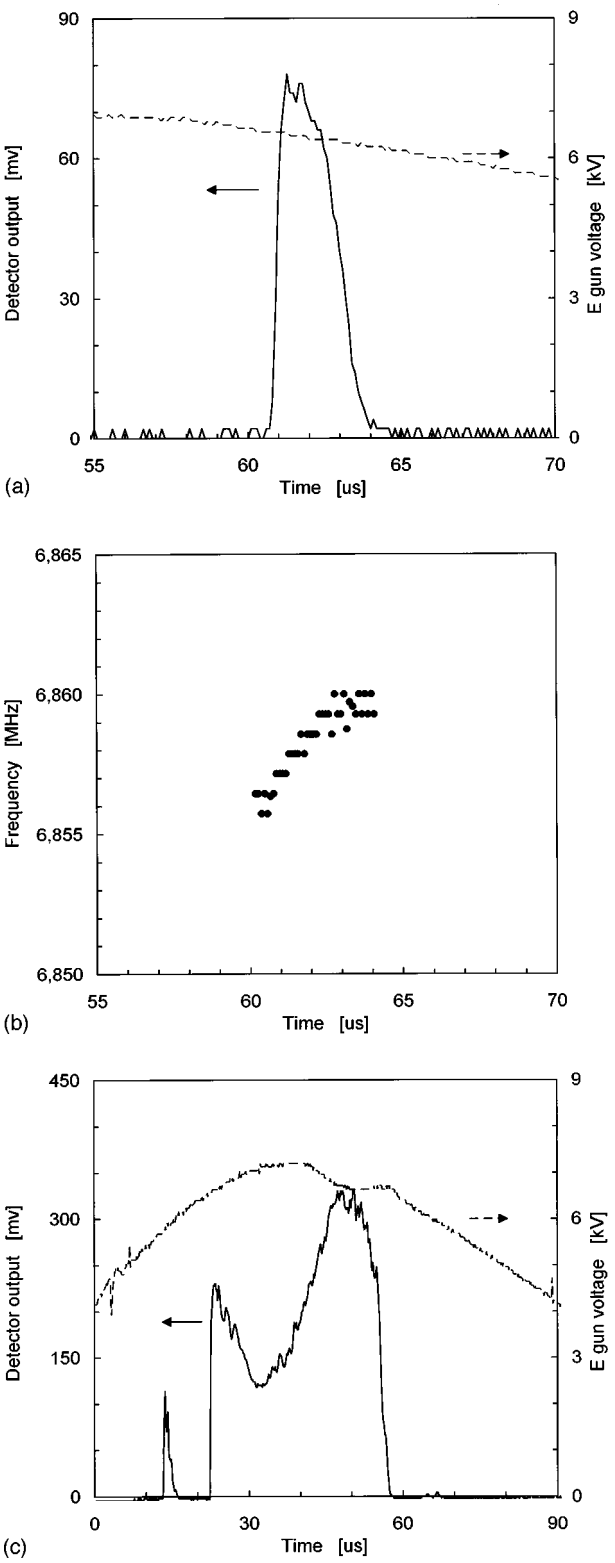

FIG. 8. Two-beam CRM oscillator output at 2.7 kG: (a) the detector output (solid line) and the electron-gun voltage (dashed line), (b) the frequency variation during the pulse, and (c) an off-tuned operation.

pulse frequency variation in this case. The corresponding cyclotron frequency is 10.5 GHz and the radiation frequency is 6.7 GHz. This result was obtained without a kicker field (as in the anomalous CRM interaction [13]).

A series of measurements was made in different electron-gun voltages in axial magnetic fields of 2.7 and 3.8 kG (7.5- and 10.5-GHz cyclotron frequencies, respectively). For 2.7 kG, the corresponding wave frequency is around 6.9 GHz and the sampled output power by the probe is ~20 W. For an axial magnetic field of 3.8 kG, the interaction occurs around 6.7 GHz without a kicker and the sampled output power is ~6 W. Maps of frequency vs electron energy accumulated in many runs are shown in Figs. 10(a) and 10(b) for 2.7 and 3.8 kG, respectively (note that each dot presents average values of the corresponding run). The electron energy acceptance for 2.7 kG is much larger than for 3.8 kG, presumably because of the smaller Doppler shift.

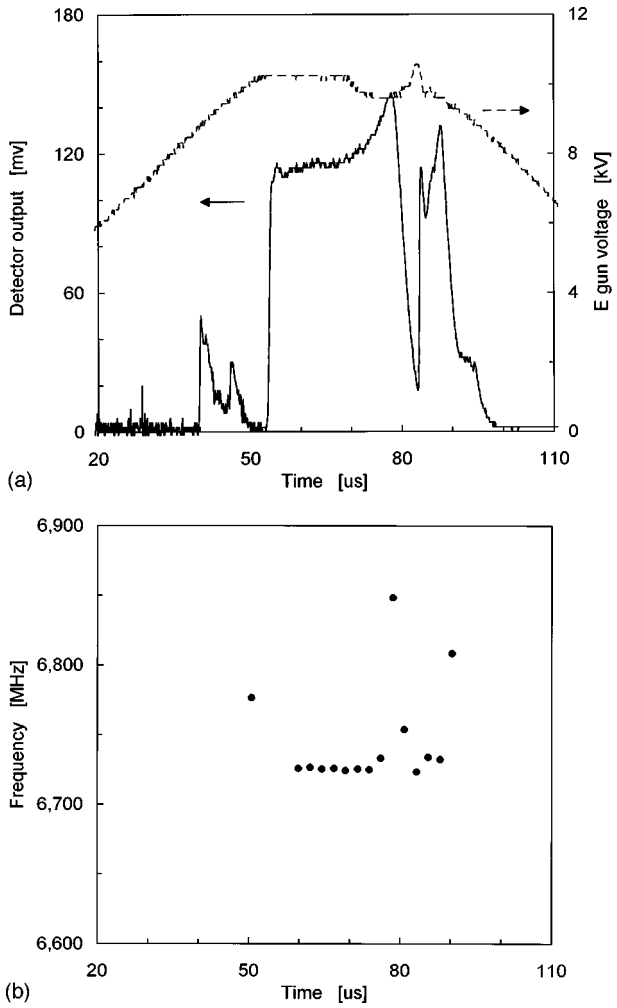

FIG. 9. Two-beam CRM operation at high magnetic field, 3.8 kG: (a) the detected rf output (solid line) and the electron-gun voltage (dashed line) and (b) the frequency variation.

The theoretical tuning condition of the CRM interaction (1) and the Brillouin dispersion diagram of Fig. 3 are applied to analyze the experimental results. The synchronism conditions observed in the two-beam 2D CRM-array experiment are illustrated in Fig. 11. The electron-beam lines are computed by Eq. (1) for 2.7 and 3.8 kG and electron energies of 6.5 and 10.2 keV, respectively. The intersection points between the electron-beam lines and the waveguide dispersion curves indicate the CRM resonance frequencies. One intersection point (at 2.7 kG) is in the fast-wave region, whereas the other (at 3.8 kG) is in the slow-wave region. Both interactions occur with backward waves.

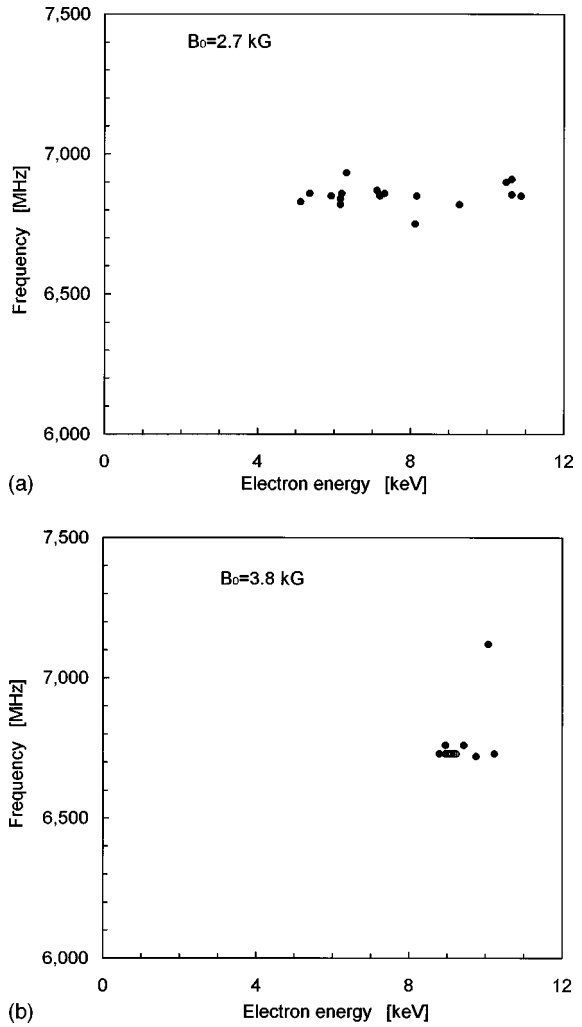

FIG. 10. Maps of frequency vs electron energy accumulated in many runs around (a) 2.7-kG and (b) 3.8-kG magnetic fields (each dot represents the average of a single run).

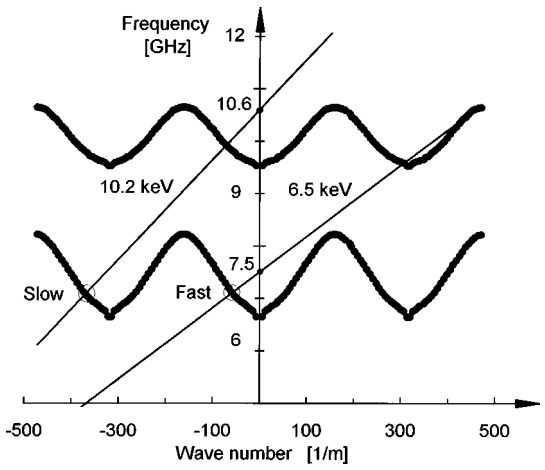

FIG. 11. Tuning-diagram presentation of Eq. (1) with the waveguide dispersion (Fig. 3) for the two-beam CRM-array results. The electron-beam lines for 6.5 keV, 2.7 kG and 10.2 keV, 3.8 kG show CRM interactions with fast and slow backward waves, respectively.

V. CONCLUSIONS

This paper presents a CRM experiment in a 2D array. The CRM tuning results indicate clearly interactions with backward waves and with fast and slow spatial harmonics of the periodic structure. The two-beam interactions occur near the cutoff frequency of the first passband. The tuning condition for the fundamental harmonic interaction leads to a wide electron energy acceptance, as observed in this experiment [note the ~6-keV spread in Fig. 10(a)].

The results of the two-beam CRM experiment show the feasibility of splitting the electron current to separate beams in the array. The same approach leads to the construction of an advanced CRM-array experiment in our laboratory [2D and 3D arrays of five (carbon-fiber) and nine (thermionic) cathodes, respectively]. Further studies proposed [3] for the development of the multibeam CRM-array concept include (a) a radiation power extraction and efficiency measurements, (b) an investigation of coupling effects between several electron beams in a 2D array, (c) development of large 3D CRM arrays, and (d) studies of direct radiation from CRM arrays, active phased-array antenna features, and radiation steering.

ACKNOWLEDGMENTS

The authors thank A. Shahadi, M. Korol, and M. Bensal for their help. This work was supported in part by the Israeli Ministry of Energy and the Belfer Center of Energy Research and by the Israeli Academy of Science and Humanities.

[1] V. A. Flyagin, A. V. Gaponov, M. I. Petelin, and V. K. Yulpatov, IEEE Trans. Microwave Theory Tech. **25**, 514 (1977).

[2] V. L. Granatstein, in *High-Power Microwaves*, edited by V. L. Granatstein and I. Alexeff (Artech, Norwood, MA, 1987), and references therein.

[3] E. Jerby (unpublished).

[4] E. Jerby, M. Korol, L. Lei, V. Dikhtiar, R. Milo, and I. Mastovsky, in *Digest of the 22nd International Conference on Infared and Millimeter Waves, Wintergreen, VA, 1997*, edited by H. P. Freund and G. Nusinovich (University of Maryland, College Park, 1998), pp. 65 and 66.

[5] M. Korol and E. Jerby, Phys. Rev. E **55**, 5934 (1997), and references therein.

[6] A. Kesar and E. Jerby, in *Digest of the International Research Workshop on CRMs and Gyrotrons, Ma'ale Hachamisha, Israel, 1998*, edited by E. Jerby and G. Nusinovich (Tel Aviv University, Ramat Aviv, Israel, 1998), p. 48; see also A. Kesar and E. Jerby, Phys. Rev. E **59**, 2465 (1999).

[7] E. A. Gelvich, L. M. Borisov, Y. V. Zhary, A. D. Zakurdayev, A. S. Pobedonostsev, and V. I. Poognin, IEEE Trans. Microwave Theory Tech. **41**, 15 (1993), and references therein.

[8] R. B. Palmer, R. C. Fernow, J. Fischer, J. C. Gallardo, H. G. Kirk, S. Ule, H. Wang, Y. Zhao, K. Eppley, W. Herrmanns-

feldt, R. Miller, and D. Yu, Nucl. Instrum. Methods Phys. Res. A **366**, 1 (1995).
[9] G. Bekefi, J. Appl. Phys. **71**, 4128 (1992).
[10] G. S. Nusinovich, B. Levush, and B. G. Danly, in *Digest of the 22nd International Conference on Infrared and Millimeter Waves* (Ref. [4]), pp. 243 and 244.
[11] K. R. Chu, A. K. Ganguly, V. L. Granatstein, J. L. Hirshfield, S. Y. Park, and J. M. Baird, Int. J. Electron. **51**, 493 (1981).
[12] T. H. Kho and A. T. Lin, Phys. Rev. A **38**, 2883 (1988).
[13] M. Einat and E. Jerby, Phys. Rev. E **56**, 5996 (1997).
[14] K. R. Chu and J. L. Hirshfield, Phys. Fluids **21**, 461 (1978), and references therein.
[15] E. Jerby and G. Bekefi, Phys. Rev. E **48**, 4637 (1993).
[16] E. Jerby, A. Shahadi, V. Grinberg, V. Dikhtyar, E. Agmon, H. Golombek, V. Trebich, M. Bensal, and G. Bekefi, IEEE J. Quantum Electron. **31**, 970 (1995).
[17] E. Jerby, Phys. Rev. E **49**, 4487 (1994).
[18] M. Korol and E. Jerby, Nucl. Instrum. Methods Phys. Res. A **375**, 222 (1996).
[19] L. Lei and E. Jerby, Proc. SPIE **2843**, 30 (1996).
[20] V. Dichtiar and E. Jerby (unpublished).
[21] H. Guo, Y. Carmel, W. R. Lou, L. Chen, J. Rodgers, D. K. Abe, A. Bromaborsky, W. Destler, and V. L. Granatstein, IEEE Trans. Microwave Theory Tech. **40**, 2086 (1992).
[22] M. Korol and E. Jerby (unpublished).